JBC ARTICLE

# Kinetic analyses of single-stranded break repair by human DNA ligase III isoforms reveal biochemical differences from DNA ligase I

Received for publication, July 7, 2017, and in revised form, July 21, 2017 Published, Papers in Press, July 27, 2017, DOI 10.1074/jbc.M117.804625

**Justin R. McNally and Patrick J. O'Brien**[1]

*From the Department of Biological Chemistry, Michigan Medicine, University of Michigan, Ann Arbor, Michigan 48109*

Edited by Patrick Sung

**Humans have three genes encoding DNA ligases with conserved structural features and activities, but they also have notable differences. The *LIG3* gene encodes a ubiquitous isoform in all tissues (LIG3$\alpha$) and a germ line–specific splicing isoform (LIG3$\beta$) that differs in the C-terminal domain. Both isoforms are found in the nucleus and the mitochondria. Here, we determined the kinetics and thermodynamics of single-stranded break ligation by LIG3$\alpha$ and LIG3$\beta$ and compared this framework to that of LIG1, the nuclear replicative ligase. The kinetic parameters of the LIG3 isoforms are nearly identical under all tested conditions, indicating that the BRCA1 C terminal (BRCT) domain specific to LIG3$\alpha$ does not alter ligation kinetics. Although LIG3 is only 22% identical to LIG1 across their conserved domains, the two enzymes had very similar maximal ligation rates. Comparison of the rate and equilibrium constants for LIG3 and LIG1 nevertheless revealed important differences. The LIG3 isoforms were seven times more efficient than LIG1 at ligating nicked DNA under optimal conditions, mainly because of their lower $K_m$ value for the DNA substrate. This could explain why LIG3 is less prone to abortive ligation than LIG1. Surprisingly, the affinity of LIG3 for $Mg^{2+}$ was ten times weaker than that of LIG1, suggesting that $Mg^{2+}$ availability regulates DNA ligation *in vivo*, because $Mg^{2+}$ levels are higher in the mitochondria than in the nucleus. The biochemical differences between the LIG3 isoforms and LIG1 identified here will guide the understanding of both unique and overlapping biological roles of these critical enzymes.**

Human DNA ligases I (LIG1), III (LIG3), and IV (LIG4) catalyze the ultimate steps in DNA replication and repair pathways. All three of the *LIG* genes are required for mouse embryonic development (1–5), and clinical mutations have been identified in both *LIG1* and *LIG4* genes that cause immunodeficiencies (6–8). LIG1 is believed to be the primary nuclear replicative DNA ligase; however, recent studies indicate that LIG1 and nuclear LIG3 have overlapping functions (9–12). The LIG3 proteins are translated from two start sites to generate mitochondrial and nuclear isoforms, the latter of which is suggested to be dispensable (10, 11, 13–16). Two alternative splice isoforms of LIG3 are known that differ in their C-terminal regions. The major LIG3 isoform (LIG3$\alpha$) contains a C-terminal BRCA1 C terminal (BRCT)[2] domain that has been shown to interact with XRCC1 (17–21). Alternative splicing in male germ cells (22, 23) gives rise to a shorter isoform (LIG3$\beta$) that lacks the BRCT domain (Fig. 1*A*). Although the beneficial roles of nuclear LIG3 isoforms are not clear, LIG3 has been implicated in error-prone alternative end joining, which can lead to chromosomal translocations (11, 24) and telomere fusions (25, 26). Furthermore, elevated levels of LIG3 have been detected in cancer, making LIG3 a candidate for anticancer therapeutics (27–30).

Crystal structures of the human DNA ligases (31, 32) show a conserved catalytic core made up of three distinct domains that encircle the substrate (Fig. 1*B*). However, the N- and C-terminal extensions differ significantly, and these regions of the protein are likely to contribute to physiological differences between the ligases (Fig. 1*A*). LIG1 has an unstructured N-terminal region that facilitates protein-protein interactions (31, 33), but this region is dispensable for ligase activity *in vitro* (31, 34). LIG3 also has an N-terminal extension containing a unique zinc-finger (ZnF) domain that has been implicated in DNA binding (32, 35–40). Furthermore, this ZnF domain has been hypothesized to be a "nick sensor" responsible for increasing LIG3 specificity and affinity toward DNA substrates containing a single-stranded DNA break (19, 32, 35, 38). The C-terminal extension of LIG3$\alpha$ contains a BRCT domain that is constitutively bound to XRCC1 in the nucleus. Because XRCC1 is not found in the mitochondria, it is of interest to characterize the biochemical properties of LIG3$\alpha$ in the absence of XRCC1 (41).

The human DNA ligases employ a conserved three-step chemical mechanism (Fig. 1*C*) to harness the energy of ATP to catalyze the formation of a phosphodiester bond between adjacent 3′-hydroxyl and 5′-phosphate groups in DNA (42). During the first chemical step of ligation (step 1), ligase catalyzes the transfer of AMP from ATP to the active-site lysine forming an

This work was supported by the Rackham Merit Fellowship from the Rackham Graduate School, a graduate student research award from Department of Biological Chemistry, and Pharmacological Sciences Training Program Grant T32GM007767. The authors declare that they have no conflicts of interest with the contents of this article. The content is solely the responsibility of the authors and does not necessarily represent the official views of the National Institutes of Health.

This article contains supplemental Figs. S1–S6.

[1] To whom correspondence should be addressed: Department of Biological Chemistry, Michigan Medicine, 1150 W. Medical Center Dr., 5301 MSRB 3, Ann Arbor, MI 48109-0600. Tel.: 734-647-5821; Fax: 734-764-3509; E-mail: pjobrien@umich.edu.

[2] The abbreviations used are: BRCT, BRCA1 C terminal; ZnF, zinc finger; DBD, DNA-binding domain; NTase, nucleotidyltransferase; OB-fold, oligonucleotide-binding fold; TCEP, tris-(2-carboxyethyl) phosphine.

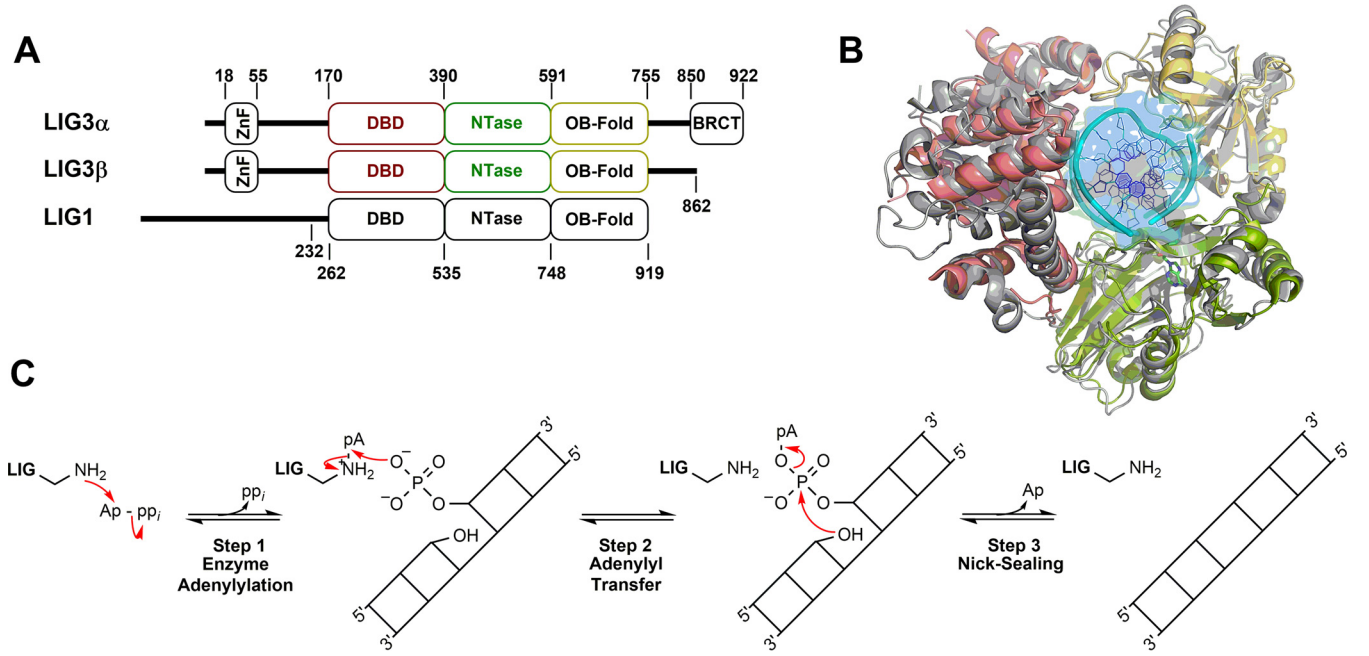


**Figure 1. Conserved structure and mechanism of human DNA ligases.** *A*, schematic representation of human DNA LIG3$\alpha$, LIG3$\beta$ and LIG1. The *numbers* indicate domain boundaries of the enzymes. LIG3$\alpha$ contains a C-terminal BRCT domain. The LIG1 $\Delta$232 truncation mutant used throughout this study is catalytically identical to full-length LIG1 (34). LIG3 isoforms and LIG1 possess conserved DBDs, NTase domains, and OB-fold domains. *B*, PyMOL (48) rendered superimposition of LIG1 (*gray*) and LIG3 (color-coded; DBD, *red*; NTase, *green*; OB-fold, *yellow*) structures with Protein Data Bank codes 1X9N and 3L2P, respectively (31, 32). *C*, mechanism of ATP-dependent DNA ligases.

adenylylated enzyme intermediate and releasing inorganic pyrophosphate. The adenylylated enzyme binds to a DNA substrate containing a single-stranded break and, during the second chemical step, catalyzes the transfer of the AMP group to the 5′-phosphate at the break (nick), thereby generating an adenylylated DNA intermediate. During step 3, the 3′-hydroxyl at the nick attacks the adenylylated 5′-phosphate to generate a new phosphodiester bond and release AMP (Fig. 1*C*). All three of these chemical steps are dependent on divalent metal ions (presumably $Mg^{2+}$), and previous work has supported a two–metal ion mechanism for step 1 (enzyme adenylylation) catalyzed by human LIG1 (34).

As a starting point for understanding the biochemical differences between LIG1 and LIG3, we describe the kinetic and thermodynamic framework for LIG3-catalyzed ligation of a single-stranded break. LIG3$\alpha$ and LIG3$\beta$ exhibit similar kinetic parameters under all tested conditions, indicating that the C-terminal BRCT domain of LIG3$\alpha$ does not directly contribute to ligation of nicked DNA substrates. Comparison of the biochemical properties of LIG3 and LIG1 reveals similar rates of the three chemical steps under conditions of saturating $Mg^{2+}$, but LIG3 has a higher $k_{cat}/K_m$ value for nicked DNA and does not release adenylylated DNA intermediates as readily as LIG1. Unexpectedly, we found that LIG3 does not bind $Mg^{2+}$ as tightly as LIG1, and this weaker binding by LIG3 is most pronounced in the nick-sealing step of catalysis. The apparent $Mg^{2+}$ affinity of ~6 mM required for the stimulation of steady-state ligation catalyzed by LIG3 suggests that LIG3 activity can be regulated by the availability of free $Mg^{2+}$, which is typically between 0.2 and 1 mM in the nucleus and cytosol (43). Intriguingly, mitochondrial $Mg^{2+}$ concentration has been reported to be 10-fold greater than cytosolic $Mg^{+2}$ levels (44), which could contribute to higher LIG3 activity in the mitochondria where it is the sole DNA ligase. This kinetic and thermodynamic framework for LIG3 identifies the different biochemical properties that distinguish it from LIG1, and it will enable future studies investigating the roles of isoform-specific accessory proteins and their contributions to ligase activity.

## Results

### *Purity, stability, and adenylylation state of the LIG3 isoforms*

Recombinant human DNA LIG3$\alpha$ and LIG3$\beta$ were purified to homogeneity over four chromatographic steps: phosphocellulose, $Ni^{2+}$–nitrilotriacetic acid, Cibacron Blue, and gel filtration (Fig. 2*A*). LIG3$\alpha$ and LIG3$\beta$ eluted at the same salt concentration from the Cibacron Blue (HiTrap Blue) column but eluted at different volumes with gel filtration, consistent with the greater molecular weight of LIG3$\alpha$. Prior to detailed kinetic studies, the stabilities of LIG3$\alpha$ and LIG3$\beta$ were investigated at 4 and 37 °C using a gel-based DNA ligation assay (supplemental Fig. S1). Both LIG3$\alpha$ and LIG3$\beta$ maintain activity when stored at 4 °C for more than 1 month (supplemental Fig. S2*A*). LIG3$\beta$ is quite stable at 37 °C ($t_{1/2} \gg 4$ h); however, LIG3$\alpha$ is significantly less stable at this temperature ($t_{1/2} = 2$ h; supplemental Fig. S2*B*). These findings are consistent with previous reports suggesting LIG3$\alpha$ is less stable than LIG3$\beta$ (45). Nevertheless, the stability studies established that both LIG3 isoforms are sufficiently stable for rigorous biochemical analysis.

Consistent with a previous report from the Ellenberger lab, we obtained a mixture of adenylylated and deadenylylated recombinant LIG3 from our initial four-step purification scheme (36). Adenylylated enzyme can be quantified by performing ligation reactions in the absence of ATP, because

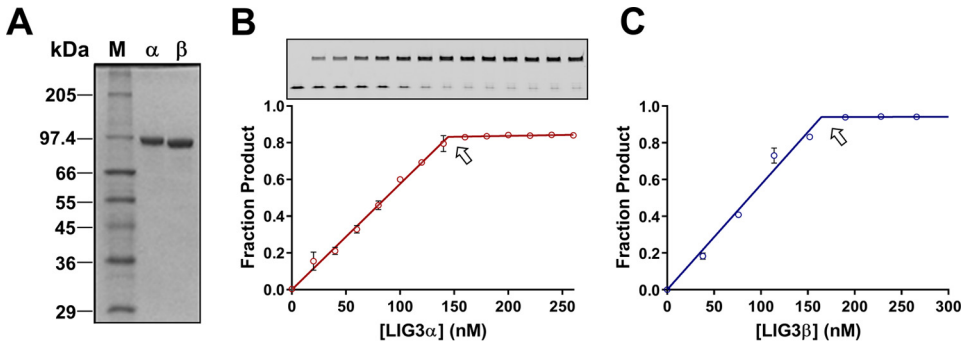


**Figure 2. Purity and active site titrations of LIG3 isoforms.** *A*, 12% SDS-PAGE gel containing 0.5 $\mu$g of purified LIG3$\alpha$ and LIG3$\beta$ with molecular masses of 102.7 and 95.9 kDa. *M*, protein sizing standards; $\alpha$, Lig3$\alpha$; $\beta$, Lig3$\beta$. *B* and *C*, representative active site titrations of LIG3$\alpha$ and LIG3$\beta$ isoform, *inset* gel shows product (*upper bands*) and substrate (*lower bands*). In the absence of ATP, the adenylylated enzyme is limited to a single turnover ligation. Reactions contained 150 nM 28-mer nicked DNA substrate and 20 mM $Mg^{2+}$ (see "Experimental procedures" for details). The equivalence point of the titration (denoted by *arrow*) indicates the concentration of adenylylated enzyme (data points are the means ± S.D.; $n = 2$).

the number of ligated DNA molecules corresponds to the number of active adenylylated enzyme molecules (Fig. 2, *B* and *C*). To assess the adenylylation status of our initial LIG3 preparations, enzyme samples were preincubated with ATP and $MgCl_2$ to fully adenylylate any deadenylylated enzyme species prior to the addition of the DNA substrate (Fig. 3*A*). Under these conditions a pre–steady-state burst was observed followed by a slower steady-state phase (Fig. 3, *B–E*). Comparison of the burst amplitude with the amplitude of ligation in the absence of ATP allowed us to determine that the preparations of LIG3$\alpha$ and LIG3$\beta$ were 73 and 81% adenylylated, respectively (Fig. 3, *B* and *C*). The heterogeneity in adenylylation status of the purified ligases was remedied in future purification protocols by treating LIG3 fractions with excess ATP and $MgCl_2$ prior to the final gel filtration step of purification (Fig. 3, *D* and *E*). The LIG3 proteins used in all subsequent experiments were purified using the improved protocol that yields homogeneous adenylylated enzyme.

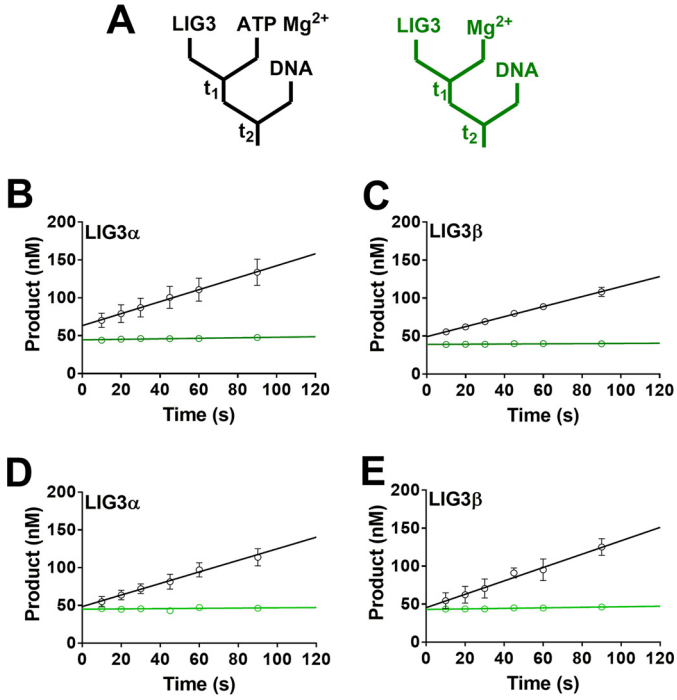


**Figure 3. Adenylylation state of purified LIG3 isoforms.** *A*, schematics for burst experiments. The *left* (*black*) scheme indicates that LIG3 was incubated in the presence of ATP and $Mg^{2+}$ to ensure complete enzyme adenylylation prior to the addition of DNA. The scheme to the *right* (*green*) displays reaction conditions in which no ATP was added to the reaction solution. The colors of the diagrams correspond to the colors of the linear fits in *B–E*. *B* and *C*, burst kinetics indicate LIG3$\alpha$ and LIG3$\beta$ are 73 and 81% adenylylated, respectively. *D* and *E*, burst kinetics of LIG3$\alpha$ and LIG3$\beta$, respectively, after the addition of an adenylylation step during protein purification generates 100% adenylylated protein. Burst experiments after preincubation of LIG3 with ATP and $Mg^{2+}$ did not increase burst amplitude. All experiments contained an estimated 50 nM enzyme, 200 nM DNA, and 20 mM $Mg^{2+}$ in the presence and absence of 0.5 $\mu$M ATP. Each experiment was completed in triplicate (means ± S.D.).

### *Substrate dependence of the LIG3 isoforms*

Steady-state conditions were used to investigate the substrate dependence of both LIG3 isoforms. The ATP concentration dependences for multiple-turnover ligation were determined in the presence of saturating $Mg^{2+}$ (20 mM) and saturating nicked DNA substrate (1 $\mu$M). The reaction progress curves generated at each ATP concentration were linear in all cases (Fig. 4*A*), and the initial rates were plotted as a function of ATP concentration (Fig. 4*B*). Fitting the Michaelis–Menten equation (Equation 1) to the ATP dependence data yielded almost identical $k_{cat}$ and $K_{m,\ ATP}$ values for LIG3$\alpha$ and LIG3$\beta$ (Table 1). These $K_m$ values are roughly 3-fold higher than the previously reported value for LIG1 that was obtained under similar reaction conditions (34).

We next examined the concentration dependence of the nicked DNA substrate, keeping fixed saturating concentrations of ATP (1 mM) and $Mg^{2+}$ (20 mM). Under the standard conditions of 150 mM ionic strength, LIG3$\beta$ saturated at a very low concentration of DNA ($K_m \leq 5$ nM; supplemental Fig. S3). It was not possible to test lower concentrations of DNA using the gel-based fluorescence assay, and therefore the salt concentration was increased to 300 mM to weaken the protein-DNA interaction. At this higher salt condition, complete Michaelis–Menten curves were obtained for both of the LIG3 isoforms (Fig. 4*C*). LIG3$\alpha$ and LIG3$\beta$ have $K_m$ values for DNA of ~60 and ~50 nM and catalytic efficiency ($k_{cat}/K_m$) values of $8.4 \times 10^6$ and $1.0 \times 10^7$ $M^{-1}$ $s^{-1}$, respectively (Table 1). The very similar rate constants observed for the two LIG3 isoforms indicate that the C-terminal BRCT domain of LIG3$\alpha$ does not directly affect the ligation reaction. To compare the catalytic efficiency of LIG3 isoforms to that of LIG1, it was necessary to determine the DNA concentration dependence of LIG1 at the same higher

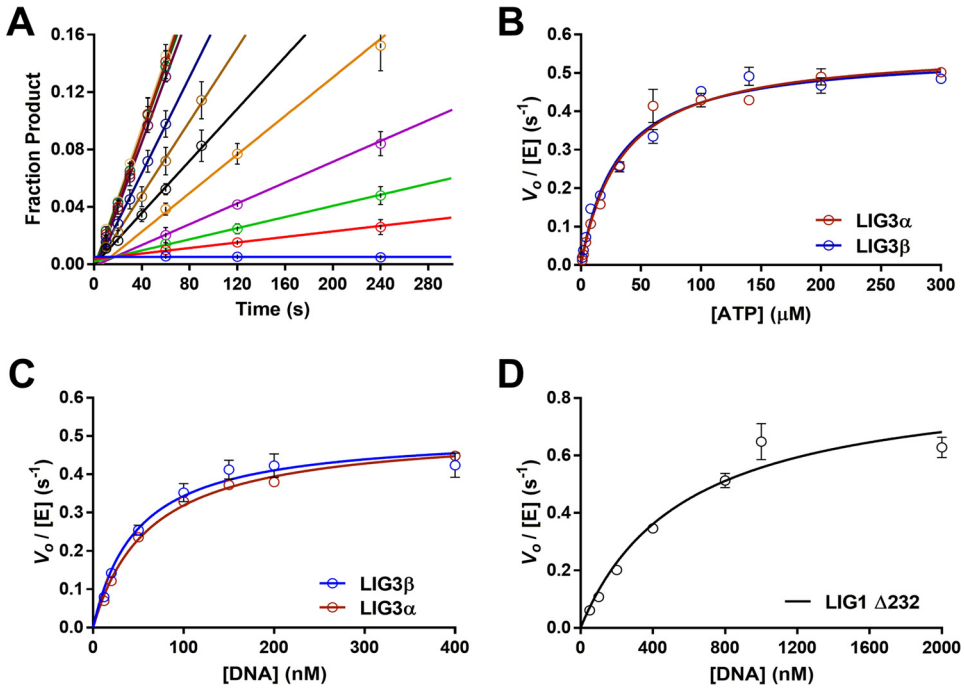


**Figure 4. Substrate dependence of LIG3α, LIG3β, and LIG1.** *A*, representative ATP concentration dependence of LIG3β used to determine initial velocities under multiple-turnover conditions. Reactions performed at each ATP concentration (0–300 μM) were fit using linear regression to determine initial rates. *B*, ATP dependence was measured under multiple-turnover conditions in the presence of saturating DNA (1 μM) and $Mg^{2+}$ (20 mM). Initial velocities are plotted as a function of ATP concentration and fit using the Michaelis–Menten equation yielding $k_{cat,\ ATP}$ values of 0.57 ± 0.02 and 0.55 ± 0.02 $s^{-1}$ for LIG3α and LIG3β, respectively. The respective $K_{m,\ ATP}$ values are 34 ± 4 and 31 ± 3 μM. *C*, DNA dependence was measured at 300 mM ionic strength with 1 mM ATP and 20 mM $Mg^{2+}$. LIG3α and LIG3β have $k_{cat,\ DNA}$ values of 0.52 ± 0.02 and 0.51 ± 0.03 $s^{-1}$ and $K_{m,\ DNA}$ values of 62 ± 6 and 49 ± 8 nM, respectively. *D*, LIG1 DNA concentration dependence was measured under the same condition as for LIG3 in *C*. The $k_{cat,\ DNA}$ value for LIG1 is 0.87 ± 0.10 $s^{-1}$ and the $K_{m,\ DNA}$ value is 570 ± 170 nM. Each experiment was completed in triplicate (means ± S.D.).

**Table 1**

**Comparison of kinetic parameters for multiple-turnover ligation by human DNA ligases**

Multiple-turnover parameters were obtained at 150 and 300 mM ionic strength. The ATP dependence was determined with 20 mM fixed concentration of $Mg^{2+}$, and the $Mg^{2+}$ dependence was determined with 1 mM fixed concentration of ATP.

| | LIG3α | LIG3β | LIG1[a] | Relative LIG3α/LIG3β | Relative LIG1/LIG3β |
|---|---|---|---|---|---|
| **150 mM I** | | | | | |
| $k_{cat,\ ATP}$ ($s^{-1}$) | 0.57 ± 0.02 | 0.55 ± 0.02 | 0.74 ± 0.09 | 1.0 | 1.3 |
| $k_{cat,\ Mg}$ ($s^{-1}$) | 0.69 ± 0.04 | 0.69 ± 0.03 | 0.81 ± 0.10 | 1.0 | 1.2 |
| $K_{m,\ ATP}$ (μM) | 34 ± 4 | 31 ± 3 | 11 ± 3 | 1.1 | 0.35 |
| $K_{Mg}$ (mM) | 5.6 ± 0.9 | 7.4 ± 0.7 | 0.71 ± 0.2 | 0.76 | **0.10** |
| $k_{cat}/K_{m,\ ATP}$ ($M^{-1}\ s^{-1}$) | 1.7 ± 0.2 × $10^4$ | 1.8 ± 0.2 × $10^4$ | 6.7 × $10^4$ | 0.94 | 3.7 |
| $k_{cat}/K_{Mg}$ ($M^{-1}\ s^{-1}$) | 120 ± 20 | 93 ± 10 | 1.1 ± 0.4 × $10^3$ | 1.3 | **12** |
| **300 mM I** | | | | | |
| $k_{cat,\ DNA}$ ($s^{-1}$) | 0.52 ± 0.02 | 0.51 ± 0.03 | 0.87 ± 0.10 | 1.0 | 1.7 |
| $K_{m,\ DNA}$ (nM) | 62 ± 6 | 49 ± 8 | 570 ± 170 | 1.3 | **12** |
| $k_{cat}/K_{m,\ DNA}$ ($M^{-1}\ s^{-1}$) | 8.4 ± 0.9 × $10^6$ | 1.0 ± 0.2 × $10^7$ | 1.5 ± 0.5 × $10^6$ | 0.84 | **0.15** |

[a] The LIG1 values at 150 mM NaCl were previously published (34). The error is represented as S.D. from the mean ($n \geq 3$).

ionic strength conditions (Fig. 4*D*). LIG1 is approximately an order of magnitude less efficient than LIG3 under these conditions, with a $K_{m,\ DNA}$ value of 570 nM and a $k_{cat}/K_{m,\ DNA}$ value of 1.5 × $10^6$ $M^{-1}\ s^{-1}$ (Table 1). The higher catalytic efficiencies of the LIG3 isoforms are primarily due to the decreased $K_{m,\ DNA}$ values.

### *$Mg^{2+}$ concentration dependence for multiple-turnover ligation*

The preceding experiments were performed in the presence of a high concentration of $Mg^{2+}$ (20 mM). This ensures that $Mg^{2+}$, which is an essential cofactor for DNA ligases, is saturating. Free $Mg^{2+}$ levels in the cell are typically much lower, and therefore it is important to investigate the $Mg^{2+}$ dependence on ligation (43). The free $Mg^{2+}$ concentration dependence for multiple-turnover ligation was determined in the presence of saturating ATP and nicked DNA substrate (1 mM ATP, 1 μM DNA). A hyperbolic one site-specific binding equation (Equation 2) fit well to the data, providing the half-maximal concentration of free $Mg^{2+}$ ($K_{Mg}$) required for ligase activity. Free $Mg^{2+}$ concentrations were calculated using the $K_d$ values for ATP·$Mg^{2+}$ and ATP·2$Mg^{2+}$. It is likely that $K_{Mg}$ is equal to the $K_d$ for $Mg^{2+}$ binding to the enzyme, because dissociation equilibrium constants in the millimolar range are typically indicative of fast dissociation rate constants. The observation that LIG3 is rapidly and efficiently quenched using EDTA on the millisecond time scale is consistent with fast dissociation of $Mg^{2+}$. The $Mg^{2+}$ dependences of LIG3α and LIG3β are essentially superimposable, and the fits yield similar $k_{cat,\ Mg}$ and $K_{Mg}$ values (Fig. 5*A* and Table 1). It is striking that the affinity for

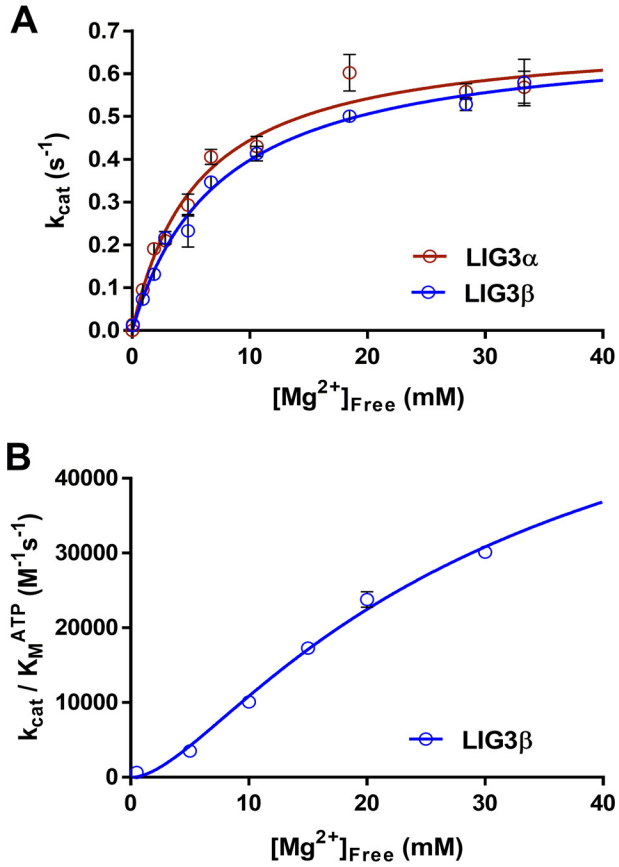


**Figure 5. Magnesium dependence for multiple-turnover ligation.** *A*, reactions contained 1 $\mu$M DNA, 1 mM ATP, and the concentration of free $Mg^{2+}$ was varied between 0 and 35 mM. The data were fit using a hyperbolic one site-specific binding equation (Equation 2) yielding maximal $k_{cat,\,Mg}$ values of 0.69 ± 0.04 and 0.69 ± 0.03 $s^{-1}$ and $K_{Mg}$ values of 5.6 ± 0.9 and 7.4 ± 0.7 mM for LIG3$\alpha$ and LIG3$\beta$, respectively. *B*, investigation of the $Mg^{2+}$ concentration dependence of enzyme adenylylation. The $Mg^{2+}$ concentration dependence was performed using subsaturating ATP concentrations (supplemental Fig. S4). The magnesium concentration dependence of $(k_{cat}/K_m)^{ATP}$ for LIG3$\beta$ was fit using a two metal random binding model (Equation 3). Each experiment was completed in at least triplicate (means ± S.D.).

$Mg^{2+}$ ($K_{Mg}$ = ~6 mM) is ~10-fold weaker than was previously observed for LIG1 under similar conditions (Table 1).

We next determined the catalytic efficiency $(k_{cat}/K_m)^{ATP}$ for LIG3$\beta$ as a function of $Mg^{2+}$ concentration, which monitors the steps up to and including enzyme adenylylation. This can be most conveniently accomplished by measuring the linear dependence of the reaction rate as a function of ATP concentration when ATP is subsaturating (supplemental Fig. S4). The $Mg^{2+}$ dependence of $(k_{cat}/K_m)^{ATP}$ (Fig. 5*B*) could not be fit well by a hyperbolic dependence on a single essential $Mg^{2+}$ but could be better fit by a two-metal ion, random binding model (Equation 3). These data support a two-metal mechanism for the reaction of LIG3 with ATP, analogous to the two–metal ion mechanism proposed for LIG1 (34).

### *Single-turnover ligation kinetics*

Although the LIG3 isoforms exhibited very similar steady-state kinetic parameters, it is possible that larger differences could exist for steps that are not rate-limiting. Therefore, we also performed single-turnover ligation experiments using excess amounts of saturating LIG3$\alpha$ and LIG3$\beta$. As previously observed for other DNA ligases, LIG3-catalyzed single-turnover ligation followed a two-step irreversible mechanism. Simultaneous fitting of the substrate, intermediate, and product yielded the microscopic rate constants for adenylyl transfer ($k_{obs,\,transfer}$) and nick-sealing ($k_{obs,\,seal}$). At a high concentration of $Mg^{2+}$ (20 mM), LIG3$\alpha$ and LIG3$\beta$ exhibit almost identical microscopic rate constants for both steps (Fig. 6, *A* and *B*). Given the identical kinetic parameters for the two LIG3 isoforms, and the greater stability of LIG3 $\beta$, we chose to perform a comprehensive single-turnover kinetic analysis of LIG3$\beta$.

To evaluate the metal cofactor requirements for each chemical step of ligation, the $Mg^{2+}$ binding affinities and microscopic rate constants were systematically determined under single-turnover conditions. The observed rate constants for adenylyl transfer (Fig. 6*C*) and nick sealing by LIG3$\beta$ (Fig. 6*D*) are plotted as a function of $Mg^{2+}$ concentration. These data were fit by a hyperbolic dependence to yield the maximal $k_{transfer}$ and $k_{seal}$ rate constants of 0.90 and 18 $s^{-1}$, respectively (Table 2). Using the net rate constants method (Equation 5), the rate constant for enzyme adenylylation ($k_{adenylylation}$) was calculated to be 1.6 $s^{-1}$ (Table 2). The rate constants at saturating $Mg^{2+}$ for all three of the chemical steps catalyzed by LIG3$\beta$ are strikingly similar to the kinetic parameters for LIG1 that were previously obtained under similar reaction conditions. The apparent affinity for $Mg^{2+}$ in the adenylyl transfer step is only 2-fold weaker for LIG3 compared with LIG1 with $K_{Mg}$ values of 0.3 and 0.15 mM, respectively. In contrast, the $Mg^{2+}$ affinity for nick-sealing is 7-fold weaker for LIG3 as compared with LIG1 with values of 18 and 2.6 mM, respectively (Table 2).

### *Accumulation of adenylylated DNA intermediates*

Previous study of LIG1 revealed that this ligase releases adenylylated DNA intermediates under conditions of low free $Mg^{2+}$ concentration (34). LIG1 is quickly adenylylated and cannot rebind the intermediate, resulting in abortive ligation (Fig. 7*A*). The propensity for abortive ligation under $Mg^{2+}$-starved conditions was attributed to differential affinity for $Mg^{2+}$ in the adenylyl transfer and nick-sealing steps (34). Because LIG3 shows a similar reduction in $Mg^{2+}$ affinity for nick sealing as compared with adenylyl transfer steps, we investigated whether LIG3 is also susceptible to abortive ligation on a nicked DNA substrate. Guided by the previous investigation of LIG1, multiple-turnover assays were conducted in the presence of low concentration of free $Mg^{2+}$ (70-fold below $K_{Mg}$). Analogous ligation reactions using LIG1 were performed for direct comparison between the enzymes. The fraction abortive ligation was calculated for both LIG1 and LIG3$\beta$ (Equation 4 and Fig. 7*B*). Whereas 8% of attempted ligation events were aborted by LIG1, only 1% of ligation events were aborted by LIG3$\beta$. Thus, LIG3 appears to be less susceptible than LIG1 to abortive ligation of nicked DNA substrates.

## Discussion

DNA ligases I and III contain three structurally conserved domains (DBD, NTase, and OB-fold domains; Fig. 1) that each contribute to substrate binding and ligation (32). Despite this

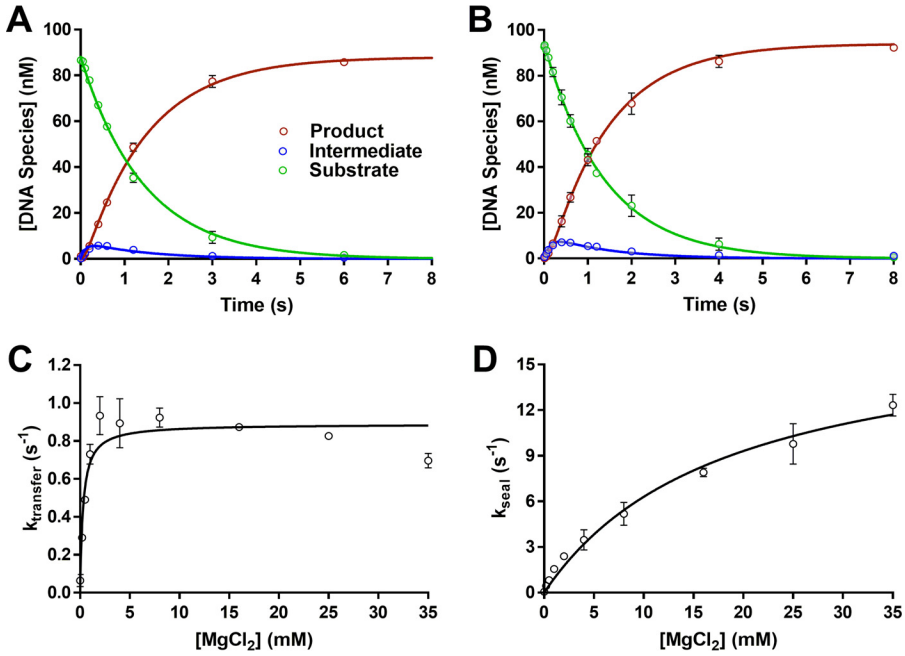


**Figure 6. Single-turnover ligation kinetics.** *A* and *B*, representative single turnover kinetics of DNA LIG3$\alpha$ (*A*) and LIG3$\beta$ (*B*) indicate the two enzymes behave similarly under single-turnover conditions at 20 mM $Mg^{2+}$. The data were fit using a two-step irreversible mechanism using the program Berkeley Madonna. The rate constants for adenylyl transfer are 0.7 and 0.8 $s^{-1}$ and for nick sealing are 8.7 and 8.9 $s^{-1}$ for LIG3$\alpha$ and LIG3$\beta$, respectively. Experiments contained 100 nM fluorescein-labeled DNA, 600 nM enzyme, and 20 mM $MgCl_2$ with no added ATP. *C*, $Mg^{2+}$ concentration dependence for the adenylyl transfer step using LIG3$\beta$. *D*, $Mg^{2+}$ concentration dependence of the nick-sealing step for LIG3$\beta$. The data were fit using a hyperbolic one site-specific binding equation (Equation 2) yielding $k_{transfer}$ and $k_{seal}$ values of 0.89 ± 0.03 and 19 ± 6 $s^{-1}$, respectively. The $K_{Mg}$ values for adenylyl transfer and nick-sealing steps are 0.30 ± 0.06 and 18 ± 3 mM, respectively. Each experiment was completed in at least triplicate (means ± S.D.).

**Table 2**

**Comparison of single-turnover parameters of LIG3$\beta$ and LIG1**

Single-turnover parameters were obtained at 150 mM ionic strength. All reactions contained 600 nM adenylylated enzyme and 100 nM nicked DNA substrate in the presence of 20 mM $Mg^{2+}$ and the absence of ATP.

| Kinetic parameter | LIG3$\beta$ | LIG1[a] | Relative LIG1/LIG3$\beta$ |
|---|---|---|---|
| $k_{adenylylation}$ ($s^{-1}$)[b] | 1.6 ± 0.2 | 1.3 ± 0.3 | 0.81 |
| $k_{transfer}$ ($s^{-1}$) | 0.89 ± 0.03 | 2.6 ± 0.6 | 2.9 |
| $k_{seal}$ ($s^{-1}$) | 19 ± 6 | 12 ± 2 | 0.63 |
| $K_{Mg,\ transfer}$ (mM) | 0.30 ± 0.07 | 0.15 ± 0.06 | 0.50 |
| $K_{Mg,\ seal}$ (mM) | 18 ± 3 | 2.6 ± 0.9 | **0.14** |

[a] LIG1 values were previously reported for Δ232 LIG1 under similar experimental conditions (34).

[b] The microscopic rate constant for enzyme adenylylation was calculated using a $k_{cat}$ value of 0.55 $s^{-1}$ with the net rate constants equation (Equation 4). The error is represented as S.D. from the mean ($n \geq 3$).

high degree of structural homology, LIG1 and LIG3 share only 22% primary sequence identity across these three domains (Fig. 1*B*). On the one hand, the high degree of structural homology might indicate similar biochemical activities, but on the other hand, there are numerous substitutions throughout the proteins, including the DNA-binding interfaces of the DBD and OB-fold domains that could lead to distinct biochemical properties. Outside of the core three-domain architecture of the ligases, the human ligases also have unique N- and C-terminal domains that likely influence their localization, protein-protein interactions, and substrate specificity. As a first step toward understanding the biochemical differences between the human DNA ligases, we have characterized recombinant human LIG3$\alpha$ and LIG3$\beta$ under single- and multiple-turnover conditions and compared the kinetic framework to that of the previously studied human DNA LIG1. This analysis reveals similarities and differences that are relevant to understanding their unique biological functions. Furthermore, this information provides an essential starting point for future studies that explore the functional consequences of mutations in LIG3, as well as the regulatory effects of LIG3 interacting proteins, such as XRCC1.

Recombinant LIG3$\alpha$ was found to be less stable than LIG3$\beta$, with a half-life of roughly 2 h, as compared with at least 4 h for LIG3$\beta$ in our assay conditions (supplemental Fig. S2). This is consistent with the previous findings by the Caldecott group (45) that LIG3$\alpha$ exhibits limited stability *in vivo* and that interaction with XRCC1 is important for stability. It remains unclear whether mitochondrial LIG3$\alpha$ requires a mitochondrial-specific protein binding partner or whether it functions as a homodimer (41). Nevertheless, the stability of recombinant Lig3$\alpha$ was sufficient for a complete *in vitro* kinetic characterization. We found that the two LIG3 isoforms are indistinguishable under all experimental conditions tested using a nicked DNA substrate (Table 1). This has implications for mitochondrial DNA ligation and establishes that the different C termini of the LIG3 isoforms do not change the kinetics of single-stranded break ligation.

We can also directly compare the kinetic parameters for the LIG3 isoforms to those of the previously studied LIG1. Comparison of the substrate dependences of the enzymes under conditions of saturating $Mg^{2+}$ demonstrates that these enzymes have very similar efficiencies for utilization of ATP. However, the LIG3 isoforms have higher catalytic efficiency than LIG1 toward nicked DNA substrates because of the reduced $K_{m,\ DNA}$ of the LIG3 isoforms. These findings are consistent with previous studies suggesting that the ZnF domain of LIG3 contributes to DNA binding during ligation of

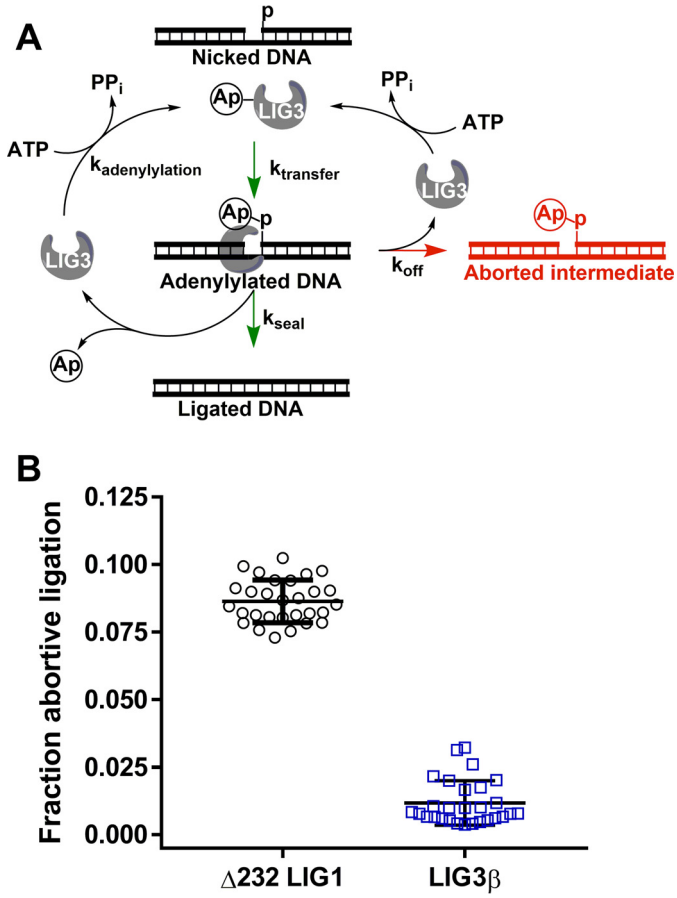


**Figure 7. Accumulation of adenylylated DNA intermediate.** *A*, abortive ligation mechanism observed under $Mg^{2+}$-starved conditions. Adenylylated ligase interacts with nicked DNA substrates, generating adenylylated DNA intermediate. The partitioning between the nick-sealing steps and abortive ligation is represented with $k_{seal}$ and $k_{off}$, respectively. Following successful or abortive ligation, ligase becomes adenylylated, preventing the enzyme from rebinding the adenylylated DNA intermediate and completing the nick-sealing step. *B*, propensity of DNA ligases for abortive ligation. Free $Mg^{2+}$ concentrations were 70-fold below $K_{Mg}$ for LIG1 and LIG3$\beta$ in all experiments. The abortive ligation data represent multiple time points obtained from multiple-turnover time courses conducted in quadruplicate (see "Experimental procedures" for details). *Error bars* indicate S.D. from the mean.

both single- and double-strand breaks (19, 32, 35, 38). A "jackknife" model for nick recognition has been previously proposed for explaining how LIG3 uses two independent DNA-binding domains to bind to a nick (32). Our studies do not directly test this model but require that the proposed conformational changes upon nick recognition would have to be fast to obtain such similar kinetics for the LIG3 isoforms and LIG1, for LIG1 lacks a ZnF domain (Fig. 1*A*). These overall similarities in the rates of the chemical steps at saturating $Mg^{2+}$ concentration are consistent with the strong conservation of the active site architecture (Fig. 1*B*).

Surprisingly, LIG3 requires a much higher concentration of $Mg^{2+}$ cofactor to achieve maximal activity as compared with LIG1. The structural basis for this biochemical difference is unknown, but the observation of an approximate 10-fold reduction in $K_{Mg}$ for steady-state ligation raises the possibility that this difference in $Mg^{2+}$ affinity is biologically relevant. The free $Mg^{2+}$ concentration in nuclei has been estimated to be between 0.2 and 2 mM, which would be subsaturating for LIG3 and lead to suppressed catalytic activity (46). In contrast, recent studies have suggested that mitochondria have up to 10-fold higher concentration of free $Mg^{2+}$ compared with the cytosol (44). We speculate that this difference in $Mg^{2+}$ affinity could reflect an adaption to limit LIG3 activity in the nucleus where multiple ligases are present and yet allow for high catalytic activity in the mitochondria where it is the sole DNA ligase.

The weaker affinity of LIG3 for $Mg^{2+}$ is most apparent in the adenylylation step and in the nick-sealing step of the reaction, whereas the adenylyl transfer step is more similar for LIG3 and LIG1 (Table 2). These differences in $Mg^{2+}$ affinity in the different steps of the reaction leads to a greater buildup of adenylylated intermediate for LIG3 (supplemental Fig. S5) as compared with LIG1 at a physiological free $Mg^{2+}$ concentration of 1 mM. Nevertheless, LIG3 is more efficient at ligation than LIG1 under conditions of low free $Mg^{2+}$, and LIG3 is not susceptible to abortive ligation on a normal nick (Fig. 7). Because abortive ligation involves the release of adenylylated DNA intermediate, we can infer that LIG3 must have greater DNA binding affinity as compared with LIG1.

## Conclusions

This study provides the foundational kinetic and thermodynamic framework for ligation of single-stranded breaks catalyzed by the LIG3 isoforms. We suggest that the BRCT domain of LIG3$\alpha$ does not contribute to ligation of single-stranded breaks, revealing nearly identical kinetic parameters for the LIG3 isoforms. The LIG3 isoforms differ from LIG1 in their substrate and $Mg^{2+}$ dependence, despite a high degree of structural similarity in the catalytic domain. The kinetic and thermodynamic framework presented here for LIG3 will facilitate future investigations of the functional differences between human DNA ligases and their variants.

## Experimental procedures

### *Expression and purification of LIG3 isoforms*

Full-length human DNA LIG3$\alpha$ and LIG3$\beta$ cDNAs were cloned into a modified pET28 plasmid containing an N-terminal $His_6$-SUMO tag, and the open reading frames were confirmed by Sanger sequencing of both strands. The enzymes were expressed in *Escherichia coli* C41 pRare 2 cells. Bacterial cultures were grown in LB and induced at an $A_{600}$ of 0.6 using 300 $\mu$M isopropyl $\beta$-D-thiogalactopyranoside followed by an incubation at 16 °C for 24 h at 230 RPM. Cells were harvested via centrifugation at 6,000 × *g* for 20 min at 4 °C. Pellets were suspended in lysis buffer (50 mM Tris, pH 7.5, 300 mM NaCl, 3 mM EDTA, 10 mM BME, 10% glycerol, 1 mM benzamidine-HCl, and 1 mM PMSF) and stored at −80 °C. Prior to purification, the cells were thawed and lysed by three passages through a cell homogenizer. Lysates were clarified by centrifugation for 1 h at 39,000 × *g* at 4 °C and further clarified using a 0.45 $\mu$m filter. All purification steps were performed at 4 °C. The clarified lysate was loaded onto a cellulose phosphate column (Sigma) equilibrated with purification buffer (50 mM Tris, pH 7.5, 10% glycerol, 2 mM BME) containing 250 mM NaCl and 3 mM EDTA. The enzyme was eluted with purification buffer containing 2 M NaCl and then loaded onto a HisTrap HP column (GE Health-

care) equilibrated with purification buffer containing 1 M NaCl and 20 mM imidazole. Loaded protein was washed using 200 mM NaCl and 20 mM imidazole and then eluted using a linear imidazole gradient of 20–600 mM. Ligase containing fractions were pooled, and the $His_6$-SUMO tag was digested using ubiquitin-like protease (ULP1) prior to loading onto a HiTrap Blue column (GE Healthcare) equilibrated with purification buffer containing 200 mM NaCl. The bound protein was eluted using a linear gradient of 200 mM to 2 M NaCl. Protein containing fractions were collected and concentrated using 30,000 molecular weight cutoff Amicon Ultra concentrators. To ensure that the purified protein was 100% adenylylated, 20 mM $MgCl_2$ and 1 mM ATP were added to the concentrated HiTrap Blue fractions and incubated for 30 min on ice. Purification buffer was exchanged with LIG3 storage buffer (50 mM NaMOPS, pH 7.5, 300 mM NaCl, 10% glycerol, 1 mM TCEP) over a Superdex S200 26/60 gel filtration column. Protein containing fractions were collected and concentrated to 40 mg/ml, snap frozen using liquid nitrogen, and stored at −80 °C. The purity of the ligase isoforms was greater than 95% as judged by SDS-PAGE (Fig. 2*A*). Human DNA ligase I (LIG1) was prepared as previously described (34).

### *DNA substrates*

Oligonucleotides were obtained from Integrated DNA Technologies and purified using 15% polyacrylamide, 8 M urea DNA sequencing gels as previously described (34). The double-stranded nicked DNA substrate used throughout this study was generated by annealing the following oligonucleotides: 5′-CCGAATCAGTCCGACGACGCATCAGCAC, 5′-GTGCTGATGCGTC, and 5′P-GTCGGACTGATTCGG-FAM, where P indicates the presence of a 5′-phosphate, and FAM indicates the presence of 3′-fluorescein. The oligonucleotides were annealed at equimolar equivalents in annealing buffer (10 mM NaMES, pH 6.5, 50 mM NaCl) by heating the solution to 95 °C and cooling to 4 °C at a rate of 12 °C/min.

### *Gel-based ligation assay*

All single- and multiple-turnover reactions were performed at 37 °C, in standard reaction buffer (50 mM NaMOPS, pH 7.5, 10% glycerol, 1 mM TCEP, 100 μg/ml BSA (MP Biomedicals)) at an ionic strength of 150 mM unless otherwise stated. Multiple-turnover ligation reactions were quenched at designated times into quench solution (90% formamide, 50 mM EDTA, 0.006% bromphenol blue, 0.006% xylene cyanol). Single-turnover experiments were quenched using 0.2 M NaOH, followed by 2-fold dilution into the quench solution described above. Quenched samples were incubated at 95 °C for 3 min, snap-cooled using ice water, and then loaded onto a 15% (w/v) polyacrylamide, 8 M urea, 1× TBE DNA denaturing gel. The gels were scanned using a Typhoon Trio$^+$ imager (GE Healthcare) set to monitor excitation at 488 nm and emission through a 520-nm band-pass filter. DNA substrate, intermediate, and product bands were quantified using ImageQuant TL (GE Healthcare). The data were plotted and analyzed using GraphPad Prism.

### *Multiple-turnover kinetics*

Steady-state reactions were performed in standard reaction buffer at 150 mM ionic strength unless otherwise stated. Multiple-turnover reaction volumes were 30 μl, from which 3 μl was quenched into 30 μl of quench solution at designated times. The initial rates were determined by the linear rate of product formation within the first 10% of product formation. The results represent the average of least three independent experiments. Burst experiments contained an estimated 50 nM ligase and 200 nM DNA. LIG3 isoforms were preincubated in the absence and presence of 20-fold greater molar concentration of ATP in the presence of 20 mM $Mg^{2+}$ for 1 h on ice followed by 10 min at 37 °C. Following the enzyme adenylylation incubations, the samples were diluted 500-fold to achieve reaction concentrations prior to mixing with DNA. The adenylylation state was determined by comparison between ATP-treated and ATP-omitted samples. Burst amplitudes are proportional to adenylylated enzyme concentration. The ATP concentration dependences of the LIG3 isoforms were investigated using 5 nM enzyme in the presence of saturating $Mg^{2+}$ (20 mM) and saturating 28-mer DNA (1 μM) while adjusting ATP concentrations between 0 and 300 μM. The initial rates ($V_0/[E]$) were plotted as a function of ATP concentration and fit using the Michaelis–Menten equation (Equation 1). The free $Mg^{2+}$ concentration dependence (0–35 mM) was investigated under both saturating and subsaturating ATP concentrations. Free $Mg^{2+}$ concentrations were calculated using $K_d$ values for ATP·$Mg^{2+}$ and ATP·$2Mg^{2+}$ of 12 μM and 17 mM as previously described (34, 47). In the presence of saturating ATP (1 mM), the initial rates were fit by a hyperbolic curve (Equation 2). In the presence of subsaturating ATP (0.5, 1, and 2 μM), $(k_{cat}/K_m)^{ATP}$ values were generated and plotted as a function of $Mg^{2+}$ concentrations revealing cooperative enzymatic behavior that best fit to a two-site random binding model (Equation 3). The DNA concentration dependence for multiple-turnover ligation was obtained using standard reaction buffer at ionic strengths of 150 and 300 mM. DNA concentration dependence values of LIG1 and LIG3 were compared under the 300 mM ionic strength reaction conditions. The reactions contained 5 nM enzyme, 1 mM ATP, 20 mM $Mg^{2+}$, and 0.02–1 μM nicked DNA substrate. Initial rates *versus* DNA concentration data were fit to the Michaelis–Menten equation (Equation 1).

$$\frac{V_{init}}{[E]} = \frac{k_{cat} \times [S]}{(K_m + [S])} \quad \text{(Eq. 1)}$$

$$\frac{V_{init}}{[E]} = \frac{k_{cat} \times [Mg^{2+}]}{(K_m + [Mg^{2+}])} \quad \text{(Eq. 2)}$$

$$\left(\frac{k_{cat}}{K_m}\right)^{ATP} = \frac{\left(\frac{k_{cat}}{K_m}\right)^{ATP}_{Max}}{\frac{K_1 \times K_2}{[Mg^{2+}]^2} + \frac{K_1 + K_2}{[Mg^{2+}]} + 1} \quad \text{(Eq. 3)}$$

### *Quantifying adenylylated DNA intermediate*

Ligation experiments were performed under multiple-turnover conditions (5 nM LIG1 or LIG3β, 200 nM nicked DNA) in

standard reaction buffer. Using LIG1 as previously described (34), the accumulation of abortive ligation intermediates was observed when free $Mg^{2+}$ concentration was 70-fold below its respective $K_{Mg}$ value. Free $Mg^{2+}$ concentrations were calculated as described above. Accumulation of abortive ligation intermediates was investigated using 1 mM $Mg^{2+}$, and the ATP concentration was adjusted to achieve a free $Mg^{2+}$ concentration that was 70-fold below the individually measured $K_{Mg}$ values for LIG1 and LIG3. 2 mM ATP was required to achieve 10.5 $\mu$M free $Mg^{2+}$ in the case of LIG1, whereas 1 mM ATP was needed to achieve 98 $\mu$M free $Mg^{2+}$ in the LIG3$\beta$ containing reactions. The fraction of aborted ligation events was calculated from the concentration of intermediate (I) and product (P) formed under the free $Mg^{2+}$-starved conditions at various points during the initial rates portion of the ligation reaction (Equation 4).

$$\text{Fraction abortive ligation} = \frac{[I]}{([I] + [P])} \qquad \text{(Eq. 4)}$$

### *Single-turnover ligation kinetics*

Single-turnover ligation kinetics were investigated using a KinTek RFQ-3 rapid mixing apparatus. Reaction times varied from 5 ms to 10 min. Experiments were performed by rapidly mixing equal volumes of 1.2 $\mu$M LIG3, and 200 nM nicked DNA substrate to generate 600 nM enzyme and 100 nM substrate. Enzyme and substrate concentrations were varied to ensure single-turnover conditions were saturating (data not shown). For experiments investigating the magnesium dependence for adenylyl-transfer and nick-sealing steps of catalysis, ionic strength was calculated using the Debye-Hückel theory of electrolytes and held constant at 150 mM using NaCl. The samples were allowed to equilibrate at 37 °C for at least 1 min prior to each reaction. Reactions were allowed to age for predetermined times and the reactions stopped using 200 mM NaOH, because the aforementioned quench solution used for multiple-turnover ligation kinetics was not sufficient to stop catalysis at 5 ms after mixing (supplemental Fig. S6). NaOH-quenched samples were diluted 2-fold in formamide quench solution and processed as previously described (34). The observed rates of adenylyl transfer and nick-sealing were plotted as a function of $Mg^{2+}$ concentration and fit using a hyperbolic single-site binding equation (Equation 2). The concentrations of total and free $Mg^{2+}$ were assumed equal because of the absence of ATP in the single-turnover reactions. The value of $k_{adenylylation}$ was calculated using the net rate constant method ($k_{cat} = 0.55\ s^{-1}$).

$$\frac{1}{k_{cat}} = \frac{1}{k_{adenylylation}} + \frac{1}{k_{transfer}} + \frac{1}{k_{seal}} \qquad \text{(Eq. 5)}$$

*Author contributions*—J. R. M. performed the experiments, J. R. M. and P. J. O. designed the study, analyzed the data, and wrote the manuscript.

*Acknowledgments—We thank T. Jurkiw for the gift of the purified Δ232 LIG1 and members of the O'Brien laboratory for helpful discussions. The University of Michigan Comprehensive Cancer Center is supported by National Cancer Institute Grant P30CA046592.*

**References**

1. Bentley, D., Selfridge, J., Millar, J. K., Samuel, K., Hole, N., Ansell, J. D., and Melton, D. W. (1996) DNA ligase I is required for fetal liver erythropoiesis but is not essential for mammalian cell viability. *Nat. Genet.* **13,** 489–491
2. Bentley, D. J., Harrison, C., Ketchen, A. M., Redhead, N. J., Samuel, K., Waterfall, M., Ansell, J. D., and Melton, D. W. (2002) DNA ligase I null mouse cells show normal DNA repair activity but altered DNA replication and reduced genome stability. *J. Cell Sci.* **115,** 1551–1561
3. Puebla-Osorio, N., Lacey, D. B., Alt, F. W., and Zhu, C. (2006) Early embryonic lethality due to targeted inactivation of DNA ligase III. *Mol. Cell Biol.* **26,** 3935–3941
4. Barnes, D. E., Stamp, G., Rosewell, I., Denzel, A., and Lindahl, T. (1998) Targeted disruption of the gene encoding DNA ligase IV leads to lethality in embryonic mice. *Curr. Biol.* **8,** 1395–1398
5. Frank, K. M., Sekiguchi, J. M., Seidl, K. J., Swat, W., Rathbun, G. A., Cheng, H. L., Davidson, L., Kangaloo, L., and Alt, F. W. (1998) Late embryonic lethality and impaired V(D)J recombination in mice lacking DNA ligase IV. *Nature* **396,** 173–177
6. Barnes, D. E., Tomkinson, A. E., Lehmann, A. R., Webster, A. D., and Lindahl, T. (1992) Mutations in the DNA ligase I gene of an individual with immunodeficiencies and cellular hypersensitivity to DNA-damaging agents. *Cell* **69,** 495–503
7. O'Driscoll, M., Cerosaletti, K. M., Girard, P. M., Dai, Y., Stumm, M., Kysela, B., Hirsch, B., Gennery, A., Palmer, S. E., Seidel, J., Gatti, R. A., Varon, R., Oettinger, M. A., Neitzel, H., Jeggo, P. A., *et al.* (2001) DNA ligase IV mutations identified in patients exhibiting developmental delay and immunodeficiency. *Mol. Cell* **8,** 1175–1185
8. Girard, P. M., Kysela, B., Härer, C. J., Doherty, A. J., and Jeggo, P. A. (2004) Analysis of DNA ligase IV mutations found in LIG4 syndrome patients: the impact of two linked polymorphisms. *Hum. Mol. Genet.* **13,** 2369–2376
9. Petrini, J. H., Xiao, Y., and Weaver, D. T. (1995) DNA ligase I mediates essential functions in mammalian cells. *Mol. Cell Biol.* **15,** 4303–4308
10. Masani, S., Han, L., Meek, K., and Yu, K. (2016) Redundant function of DNA ligase 1 and 3 in alternative end-joining during immunoglobulin class switch recombination. *Proc. Natl. Acad. Sci. U.S.A.* **113,** 1261–1266
11. Lu, G., Duan, J., Shu, S., Wang, X., Gao, L., Guo, J., and Zhang, Y. (2016) Ligase I and ligase III mediate the DNA double-strand break ligation in alternative end-joining. *Proc. Natl. Acad. Sci. U.S.A.* **113,** 1256–1260
12. Han, L., Masani, S., Hsieh, C. L., and Yu, K. (2014) DNA ligase I is not essential for mammalian cell viability. *Cell Rep.* **7,** 316–320
13. Simsek, D., Furda, A., Gao, Y., Artus, J., Brunet, E., Hadjantonakis, A.-K., Van Houten, B., Shuman, S., McKinnon, P. J., and Jasin, M. (2011) Crucial role for DNA ligase III in mitochondria but not in Xrcc1-dependent repair. *Nature* **471,** 245–248
14. Gao, Y., Katyal, S., Lee, Y., Zhao, J., Rehg, J. E., Russell, H. R., and McKinnon, P. J. (2011) DNA ligase III is critical for mtDNA integrity but not Xrcc1-mediated nuclear DNA repair. *Nature* **471,** 240–244
15. Arakawa, H., Bednar, T., Wang, M., Paul, K., Mladenov, E., Bencsik-Theilen, A. A., and Iliakis, G. (2012) Functional redundancy between DNA ligases I and III in DNA replication in vertebrate cells. *Nucleic Acids Res.* **40,** 2599–2610
16. Lakshmipathy, U., and Campbell, C. (1999) The human DNA ligase III gene encodes nuclear and mitochondrial proteins. *Mol. Cell Biol.* **19,** 3869–3876
17. Caldecott, K. W., McKeown, C. K., Tucker, J. D., Ljungquist, S., and Thompson, L. H. (1994) An interaction between the mammalian DNA repair protein XRCC1 and DNA ligase III. *Mol. Cell Biol.* **14,** 68–76
18. Caldecott, K. W., Tucker, J. D., Stanker, L. H., and Thompson, L. H. (1995) Characterization of the XRCC1-DNA ligase III complex *in vitro* and its absence from mutant hamster cells. *Nucleic Acids Res.* **23,** 4836–4843
19. Caldecott, K. W., Aoufouchi, S., Johnson, P., and Shall, S. (1996) XRCC1 polypeptide interacts with DNA polymerase $\beta$ and possibly poly(ADP-ribose) polymerase, and DNA ligase III is a novel molecular "nick-sensor" *in vitro*. *Nucleic Acids Res.* **24,** 4387–4394

20. Nash, R. A., Caldecott, K. W., Barnes, D. E., and Lindahl, T. (1997) XRCC1 protein interacts with one of two distinct forms of DNA ligase III. *Biochemistry* **36,** 5207–5211
21. Taylor, R. M., Wickstead, B., Cronin, S., and Caldecott, K. W. (1998) Role of a BRCT domain in the interaction of DNA ligase III-$\alpha$ with the DNA repair protein XRCC1. *Curr. Biol.* **8,** 877–880
22. Perez-Jannotti, R. M., Klein, S. M., and Bogenhagen, D. F. (2001) Two forms of mitochondrial DNA ligase III are produced in *Xenopus laevis* oocytes. *J. Biol. Chem.* **276,** 48978–48987
23. Mackey, Z. B., Ramos, W., Levin, D. S., Walter, C. A., McCarrey, J. R., and Tomkinson, A. E. (1997) An alternative splicing event which occurs in mouse pachytene spermatocytes generates a form of DNA ligase III with distinct biochemical properties that may function in meiotic recombination. *Mol. Cell Biol.* **17,** 989–998
24. Simsek, D., Brunet, E., Wong, S. Y., Katyal, S., Gao, Y., McKinnon, P. J., Lou, J., Zhang, L., Li, J., Rebar, E. J., Gregory, P. D., Holmes, M. C., and Jasin, M. (2011) DNA ligase III promotes alternative nonhomologous end-joining during chromosomal translocation formation. *PLoS Genet.* **7,** e1002080
25. Badie, S., Carlos, A. R., Folio, C., Okamoto, K., Bouwman, P., Jonkers, J., and Tarsounas, M. (2015) BRCA1 and CtIP promote alternative non-homologous end-joining at uncapped telomeres. *EMBO J.* **34,** 828
26. Jones, R. E., Oh, S., Grimstead, J. W., Zimbric, J., Roger, L., Heppel, N. H., Ashelford, K. E., Liddiard, K., Hendrickson, E. A., and Baird, D. M. (2014) Escape from telomere-driven crisis is DNA ligase III dependent. *Cell Rep.* **8,** 1063–1076
27. Newman, E. A., Lu, F., Bashllari, D., Wang, L., Opipari, A. W., and Castle, V. P. (2015) Alternative NHEJ pathway components are therapeutic targets in high-risk neuroblastoma. *Mol. Cancer Res.* **13,** 470–482
28. Tomkinson, A. E., Howes, T. R., and Wiest, N. E. (2013) DNA ligases as therapeutic targets. *Transl. Cancer Res.* **2,** 1219
29. Tobin, L. A., Robert, C., Nagaria, P., Chumsri, S., Twaddell, W., Ioffe, O. B., Greco, G. E., Brodie, A. H., Tomkinson, A. E., and Rassool, F. V. (2012) Targeting abnormal DNA repair in therapy-resistant breast cancers. *Mol. Cancer Res.* **10,** 96–107
30. Tobin, L. A., Robert, C., Rapoport, A. P., Gojo, I., Baer, M. R., Tomkinson, A. E., and Rassool, F. V. (2013) Targeting abnormal DNA double-strand break repair in tyrosine kinase inhibitor-resistant chronic myeloid leukemias. *Oncogene* **32,** 1784–1793
31. Pascal, J. M., O'Brien, P. J., Tomkinson, A. E., and Ellenberger, T. (2004) Human DNA ligase I completely encircles and partially unwinds nicked DNA. *Nature* **432,** 473–478
32. Cotner-Gohara, E., Kim, I.-K., Hammel, M., Tainer, J. A., Tomkinson, A. E., and Ellenberger, T. (2010) Human DNA ligase III recognizes DNA ends by dynamic switching between two DNA-bound states. *Biochemistry* **49,** 6165–6176
33. Ellenberger, T., and Tomkinson, A. E. (2008) Eukaryotic DNA ligases: structural and functional insights. *Annu. Rev. Biochem.* **77,** 313–338
34. Taylor, M. R., Conrad, J. A., Wahl, D., and O'Brien, P. J. (2011) Kinetic mechanism of human DNA ligase I reveals magnesium-dependent changes in the rate-limiting step that compromise ligation efficiency. *J. Biol. Chem.* **286,** 23054–23062
35. Cotner-Gohara, E., Kim, I.-K., Tomkinson, A. E., and Ellenberger, T. (2008) Two DNA-binding and nick recognition modules in human DNA ligase III. *J. Biol. Chem.* **283,** 10764–10772
36. Kukshal, V., Kim, I. K., Hura, G. L., Tomkinson, A. E., Tainer, J. A., and Ellenberger, T. (2015) Human DNA ligase III bridges two DNA ends to promote specific intermolecular DNA end joining. *Nucleic Acids Res.* **43,** 7021–7031
37. Taylor, R. M., Whitehouse, J., Cappelli, E., Frosina, G., and Caldecott, K. W. (1998) Role of the DNA ligase III zinc finger in polynucleotide binding and ligation. *Nucleic Acids Res.* **26,** 4804–4810
38. Mackey, Z. B., Niedergang, C., Murcia, J. M., Leppard, J., Au, K., Chen, J., de Murcia, G., and Tomkinson, A. E. (1999) DNA ligase III is recruited to DNA strand breaks by a zinc finger motif homologous to that of poly-(ADP-ribose) polymerase identification of two functionally distinct DNA binding regions within DNA ligase III. *J. Biol. Chem.* **274,** 21679–21687
39. Taylor, R. M., Whitehouse, C. J., and Caldecott, K. W. (2000) The DNA ligase III zinc finger stimulates binding to DNA secondary structure and promotes end joining. *Nucleic Acids Res.* **28,** 3558–3563
40. Tomkinson, A. E., and Sallmyr, A. (2013) Structure and function of the DNA ligases encoded by the mammalian LIG3 gene. *Gene* **531,** 150–157
41. Lakshmipathy, U., and Campbell, C. (2000) Mitochondrial DNA ligase III function is independent of Xrcc1. *Nucleic Acids Res.* **28,** 3880–3886
42. Tomkinson, A. E., Vijayakumar, S., Pascal, J. M., and Ellenberger, T. (2006) DNA ligases: structure, reaction mechanism, and function. *Chem. Rev.* **106,** 687–699
43. Romani, A. M. (2011) Cellular magnesium homeostasis. *Arch. Biochem. Biophys.* **512,** 1–23
44. Gout, E., Rébeillé, F., Douce, R., and Bligny, R. (2014) Interplay of $Mg^{2+}$, ADP, and ATP in the cytosol and mitochondria: unravelling the role of $Mg^{2+}$ in cell respiration. *Proc. Natl. Acad. Sci. U.S.A.* **111,** E4560–E4567
45. Taylor, R. M., Moore, D. J., Whitehouse, J., Johnson, P., and Caldecott, K. W. (2000) A cell cycle-specific requirement for the XRCC1 BRCT II domain during mammalian DNA strand break repair. *Mol. Cell Biol.* **20,** 735–740
46. Günther, T. (2006) Concentration, compartmentation and metabolic function of intracellular free $Mg^{2+}$. *Magnes. Res.* **19,** 225–236
47. Cherepanov, A. V., and de Vries, S. (2003) Kinetics and thermodynamics of nick sealing by T4 DNA ligase. *Eur. J. Biochem.* **270,** 4315–4325
48. DeLano, W. L. (2012) *The PyMOL Molecular Graphics System*, version 1.5.0.1, Schrödinger, LLC, New York